RSC Advances

PAPER

View Article Online
View Journal | View Issue

Check for updates

Cite this: *RSC Adv.*, 2023, **13**, 27756

Characterization of sulfur/carbon copolymer cathodes for Li–S batteries: a combined experimental and *ab initio* Raman spectroscopy study†

Rana Kiani, Matthias Steimecke, Marah Alqaisi, Michael Bron, Daniel Sebastiani and Pouya Partovi-Azar *

Optimization of lithium–sulfur batteries highly depends on exploring and characterizing new cathode materials. Sulfur/carbon copolymers have recently attracted much attention as an alternative class of cathodes to replace crystalline sulfur. In particular, poly(sulfur-*n*-1,3-diisopropenylbenzene) (S/DIB) has been under considerable experimental and theoretical investigations, promising a good performance in mitigating the so-called shuttle effect. Here, combining *ab initio* Raman spectroscopy simulations with experimental measurements, we show that S/DIB copolymers containing short and long sulfur chains are distinguishable based on their Raman activity in 400–500 cm^{-1}. This frequency range corresponds to S–S stretching vibrations and is only observed in the Raman spectra of those copolymers with longer sulfur chains. The results reported in this study have direct applications in identification and characterization of general sulfur/carbon copolymers with different sulfur contents.

Received 5th May 2023
Accepted 12th September 2023

DOI: 10.1039/d3ra02980h

rsc.li/rsc-advances

Open Access Article. Published on 18 September 2023. Downloaded on 6/18/2026 1:52:15 AM.
This article is licensed under a Creative Commons Attribution-NonCommercial 3.0 Unported Licence.

Introduction

Lithium–sulfur (Li–S) batteries are considered as one of the candidates for next-generation energy-storage devices. Despite their very high specific energy, commercialization of Li–S batteries is negatively affected by few drawbacks, such as irreversible capacity fade and volumetric expansion of the crystalline sulfur during the discharge. Recently, a huge amount of studies has been concentrated on using polymeric sulfur cathodes to overcome these problems. In particular, sulfur/carbon copolymers such as poly(sulfur-*n*-1,3-diisopropenylbenzene) (S/DIB) have attracted much attention. Thanks to a straightforward synthesis procedure,[1,2] S/DIB copolymers could be produced in large quantities relatively easily. In addition, it has been demonstrated that S/DIB copolymers show a promising performance in alleviating the shuttle effect and therefore, can result in a stable cycling performance of a Li–S battery.[3,4]

Nevertheless, to this day neither the lithiation mechanism of S/DIB copolymer cathodes has been entirely resolved at an atomistic level, nor their structural evolution during the discharge has been fully understood. A first step towards understanding the discharge mechanism of the S/DIB copolymers is to decipher their structural properties at the fully charged state of the battery, where no lithiation reaction has occurred. It has been recently found that short S_n chains ($n \simeq 4$) show a higher formation probability compared to other sulfur chain lengths. It has also been observed that the stability of S/DIB copolymers is brought about by the formation of short S chains.[5] In addition, short S chains have been predicted[6,7] and reported[8,9] to be more favorable in other sulfur/carbon copolymer materials involving organic groups interconnected *via* sulfur chains. The formation of Li-polysulfides during discharge has been shown to be largely hindered in S/DIB copolymer cathode involving short S chains and therefore, they exhibit a much better performance in terms of cycle life. It has been argued that even copolymers involving longer S chains (lower organic mass fraction), would show a tendency towards around 40% mass fraction (SDIB40) and shorter sulfur chains after cycling.[5] Therefore, a strategy for the synthesis of S/DIB copolymers as well as their structural modification is highly called for, in which the formation of S_n chains with short lengths ($n \leq 4$) has the highest probability.

However, in order to reach this goal first it must be understood how physical and chemical properties of S/DIB copolymers involving short and long sulfur chains are different. For example, vibrational spectroscopic signatures of "local" DIB-S_n-DIB structures and their contribution to the total spectra of S/DIB copolymer are not yet known. Moreover, up to now any estimation on the sulfur chain length distribution in S/DIB

Institute of Chemistry, Martin Luther University Halle-Wittenberg, Von-Danckelmann-Platz 4, 06120 Halle (Saale), Germany. E-mail: pouya.partovi-azar@chemie.uni-halle.de

† Electronic supplementary information (ESI) available: Further remarks on Raman spectroscopy simulations and measurements, structural analysis using ^{1}H NMR spectroscopy of the S/DIB copolymers. See DOI: https://doi.org/10.1039/d3ra02980h

© 2023 The Author(s). Published by the Royal Society of Chemistry

Open Access Article. Published on 18 September 2023. Downloaded on 6/18/2026 1:52:15 AM.
This article is licensed under a Creative Commons Attribution-NonCommercial 3.0 Unported Licence.

systems have been based on the sulfur (or DIB) mass fraction used in the synthesis process.[10–12] Therefore, a question which remains to be answered is whether it is possible to distinguish between short and long sulfur chains in sulfur/carbon copolymers.

In this article, we address the above question by combining experimental Raman spectroscopy measurements with *ab initio* Raman spectroscopy simulations at room temperature. Raman spectroscopy is a powerful tool for analyzing sulfur-containing materials due to strongly polarizable S–S covalent bonds. It is particularly suitable for *in situ* experiments, providing valuable insights on structural modifications during reactions and has been successfully used to study the lithiation mechanism of sulfur cathodes in Li–S batteries.[13–16] In this article, we focus on S/DIB copolymer cathodes at the fully charged state of the battery, meaning the point at which there is no ongoing reaction with lithium and the cathode material only contains the sulfur/carbon copolymer. In the next section, we introduce our computational and experimental methods as well as the synthesis procedure. This will be followed by presentation of the results and concluding remarks.

Methodology

Computational details

As it has been shown earlier,[5] DIB molecules are preferably connected *via* short sulfur chains ($n \simeq 4$). Here, we consider DIB-S_4-DIB and DIB-S_8-DIB as target molecules in vacuum, representing local structures of poly(sulfur-*n*-1,3-diisopropenylbenzene) containing short and long S chains, respectively. The connection of the sulfur chains and the DIB molecules are assumed to be *via* a quaternary carbon. For the sake of comparison, we also consider gas-phase S_4 and S_8 chains with terminal sulfur atoms saturated with hydrogens. Additionally, sulfur-free 1,3-diisopropenylbenzene and 1,3-diisopropylbenzene molecule are studied.

Following our previous work,[5] a temperature-assisted minimum-energy structure search is carried out: first, classical molecular dynamics (MD) simulations at 300 K using General Amber Force Field (GAFF)[17] as implemented in the GULP code[18–20] is performed for 10 ns in canonical ensemble. The atomic charges are calculated using the RESP method[21] at density functional theory (DFT) level employing the sphere sampling of the fitting points for molecular structures[22] together with the REPEAT method.[23] A time step of 0.5 fs is considered in all simulations while the temperature is controlled by a Nosé–Hoover thermostat.[24,25] For each system, 10 uncorrelated snapshots were extracted from the classical MD trajectories, roughly every 1 ns. Afterwards, minimum-energy structures are obtained through geometry optimizations at DFT level.

All DFT calculations are performed using the CP2K/QUICKSTEP software package[26] in conjunction with a DZVP-MOLOPT basis set,[27] as well as Perdew–Burke–Ernzerhof (PBE)[28] exchange-correlation energy functional and Geodecker–Teter–Hutter (GTH) pseudopotentials.[29,30] The semi-empirical DFT-D3 (ref. 31) method is used to correct for the long-range dispersion interactions. All calculations in this work are performed in vacuum.

The efficient Wannier polarizability method is used to simulate Raman spectra.[15,32] In this method, the mean polarizability is expressed as a sum of isotropic polarizabilities attributed to each Wannier function in the system, $\overline{A} = \beta/3 \sum_{i=1}^{N_{WF}} {S_i}^3$, where S_i are the Wannier spreads and the proportionality constant is obtained to be $\beta \simeq 0.9$. Such an expression for the mean polarizability also allows for the decomposition of the total Raman spectra into local contributions[33] and provides a straightforward way for the assignment of Raman peaks (see ESI†).

All Raman spectra are obtained by performing 20 ps *ab initio* molecular dynamics (AIMD) simulations in the canonical ensemble to achieve equilibrium at 300 K, followed by 80 ps AIMD simulations in the micro-canonical ensemble to remove thermostat effects and sample the polarizabilities. A time step of 1 fs is used in these simulations and polarizabilities are sampled every 5 fs. The AIMD simulations are also performed using the CP2K software with the same simulation setup as mentioned earlier. Power spectra have been calculated using the TRAVIS program.[34,35] The power spectra are normalized in a way that the sum of partial spectra gives the total power spectrum.

Material and synthesis

The S/DIB samples are synthesized with different weight percentages of DIB, namely 20, 25, 30, 40, and 50 wt%, following the method presented in ref. 36 and 37. Elemental solid sulfur (99.5%, Sigma Aldrich) is used without further treatment. Sulfur in the powder form is heated to 185 °C using a thermostated oil bath under the fume hood until a clear yellowish molten sulfur is formed. DIB (97%, Sigma Aldrich) is passed through an activated, basic aluminum oxide column to remove 4-*tert*-Butylcatechol (TBC) as a stabilizer. Afterwards, pure DIB is directly added through a syringe to the molten sulfur. The mixture is stirred by a magnetic stir bar for 10 minutes at 185 °C to enhance the ring-opening polymerization of sulfur and to obtain chemically stable copolymers. Afterward, each sample is placed in a vacuum oven for approximately 15 minutes at 176 °C to complete the reaction and reduce the amount of remaining monomers. Then, they are cooled down to room temperature. Within a few minutes, this results in a vitrified red polymer. We assume that the sulfur content remains nearly unchanged after the heating process since the synthesis involves heating at temperatures below the boiling point of sulfur. Additionally, the inverse vulcanization is a solvent-free synthesis procedure. This also ensures that the sulfur content is not altered during the synthesis process due to solvent evaporation. Elemental analysis on S/DIB samples also confirms the above conclusion (please see the ESI†). The samples are further investigated using NMR spectroscopy in order to confirm the formation of desired copolymers. Since low solubility of the S/DIB copolymers in organic solvents is a challenging factor, here we grind the samples using a mortar to increase sample surface, and then

Open Access Article. Published on 18 September 2023. Downloaded on 6/18/2026 1:52:15 AM. This article is licensed under a Creative Commons Attribution-NonCommercial 3.0 Unported Licence.

dissolve them in deuterated chloroform ($CDCl_3$) and place them in ultrasonication water bath to accelerate their solubility. ^1H NMR is carried out afterwards. Further information is provided in the ESI.†

Instrumentation and methods

NMR spectra are recorded using Varian Gemini 400 MHz NMR spectrometer. Deuterated chloroform is used as solvent. Chemical shifts are given in parts per million (ppm). MestReNova 14.2.1-27684 is used for spectra interpretation and analysis.

Raman spectra of all samples are recorded by a confocal Raman microscope setup (inVia, Renishaw) consisting of a 532 nm laser as excitation source, notch filter, a turnable grating (1800 lines mm^{-1}), a CCD camera and a light microscope (Leica, DMI2500). The microscope is equipped with a ×100 objective (Leica) to focus the laser spot (*ca.* 1 μm) on the sample as well as to collect the scattered Raman light. Before the measurements, the instrument is calibrated to a band at 520.4 cm^{-1} of a polycrystalline silicon disk. All samples are prepared onto a glass slide and several single spectra are recorded between 100–2000 cm^{-1}. In all cases, the laser power is adjusted to 0.1 mW and each sample spot illuminated for 10 s. Several spectra are recorded at various positions at the samples to ensure homogeneity.

Results and discussion

First, we start by calculating *ab initio* Raman spectra of a 1,3-diisopropenylbenzene (DIB) and a 1,3-diisopropylbenzene molecule at 300 K in vacuum. The Raman spectra are shown in Fig. 1a and b, respectively.

The Raman spectra presented here agree well with the previous studies,[38,39] with an overall mean relative error of about 10% in dominant peak positions. In comparison to the Raman spectrum of 1,3-diisopropenylbenzene in Fig. 1a, 1,3-diisopropylbenzene shows similar Raman activities [Fig. 1b], the main difference being the activities around 1560 and 1640 cm^{-1} related to the C=C stretching vibration in propenyl groups. The Raman activities in the range of 650–1500 cm^{-1} are mainly dominated by aromatic ring vibrations, while the activities around 3000 cm^{-1} arise from C–H stretching vibrations in both Fig. 1a and b.[40] Another difference in the Raman spectra presented in Fig. 1a and b is the activity at ∼450 cm^{-1}. This peak corresponds to a CH_3 vibration in the propyl group in 1,3-diisopropylbenzene[41] and is much less intensive in 1,3-diisopropenylbenzene spectrum (see ESI†).

Calculated Raman spectra of a DIB-S_4-DIB and a DIB-S_8-DIB at 300 K are shown in Fig. 2a and b in blue curves, respectively. For comparison, Raman spectra of isolated S_4 and S_8 chains, where the terminal S atoms are saturated with hydrogens, are also calculated. These spectra are shown in black curves in Fig. 2a and b, respectively. The red curves in Fig. 2a and b show partial Raman spectra corresponding to the vibrations of S_4 and S_8 chains within DIB-S_4-DIB and DIB-S_8-DIB structures.

Comparison between the spectra shown in black and red curves in Fig. 2a indicates that the characteristic vibrations of S_4 chain are almost fully suppressed in DIB-S_4-DIB due to the presence of DIB molecules. In particular, despite S–S bonds being present, Raman activities at ∼165 cm^{-1} and 400–500 cm^{-1}, which are assigned to S–S–S deformation and S–S stretching vibrations in free S_4 chain respectively (see ESI†), are absent in the partial spectrum of S_4 in DIB-S_4-DIB. However in Fig. 2b, although Raman activities below 200 cm^{-1} are absent in the partial spectrum of S_8 chain within DIB-S_8-DIB, a Raman peak corresponding to the characteristic S–S stretching vibration at 455 cm^{-1} is seen. Moreover, this activity appears to mainly arise from the S_8 chain between two DIBs [red curve in Fig. 2b].

To further assess the above observation, we calculate power spectra of the same systems [Fig. 2c and d]. In Fig. 2c, a peak is observed at around 450 cm^{-1} in the power spectrum of DIB-S_4-DIB system (blue curve). Note that there is no activity around 450 cm^{-1} in the partial power spectrum of the S_4 chain within DIB-S_4-DIB in Fig. 2c shown in dotted red curve. As mentioned earlier, this activity corresponds to a Raman-active CH_3 vibration in 1,3-diisopropylbenzene [Fig. 1b]. This vibration becomes Raman inactive in DIB-S_4-DIB as no Raman activity is observed around its corresponding frequency in Fig. 2a. This could be due to the fact that the change in the total polarizability due to this vibration is minimal in a DIB-S_4-DIB molecule. Moreover,

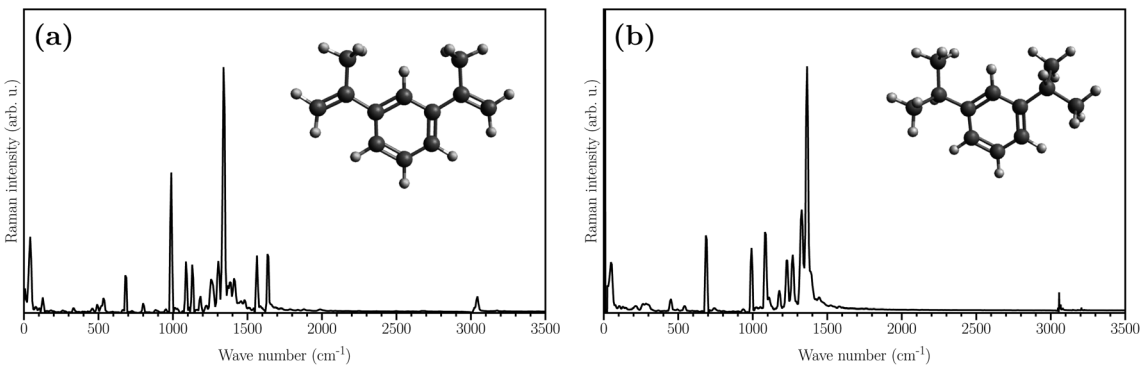

Fig. 1 Calculated Raman spectra of (a) 1,3-diisopropenylbenzene (DIB) and (b) a 1,3-diisopropylbenzene in vacuum. Corresponding atomic structures are also shown in the insets.

© 2023 The Author(s). Published by the Royal Society of Chemistry

Open Access Article. Published on 18 September 2023. Downloaded on 6/18/2026 1:52:15 AM.
This article is licensed under a Creative Commons Attribution-NonCommercial 3.0 Unported Licence.

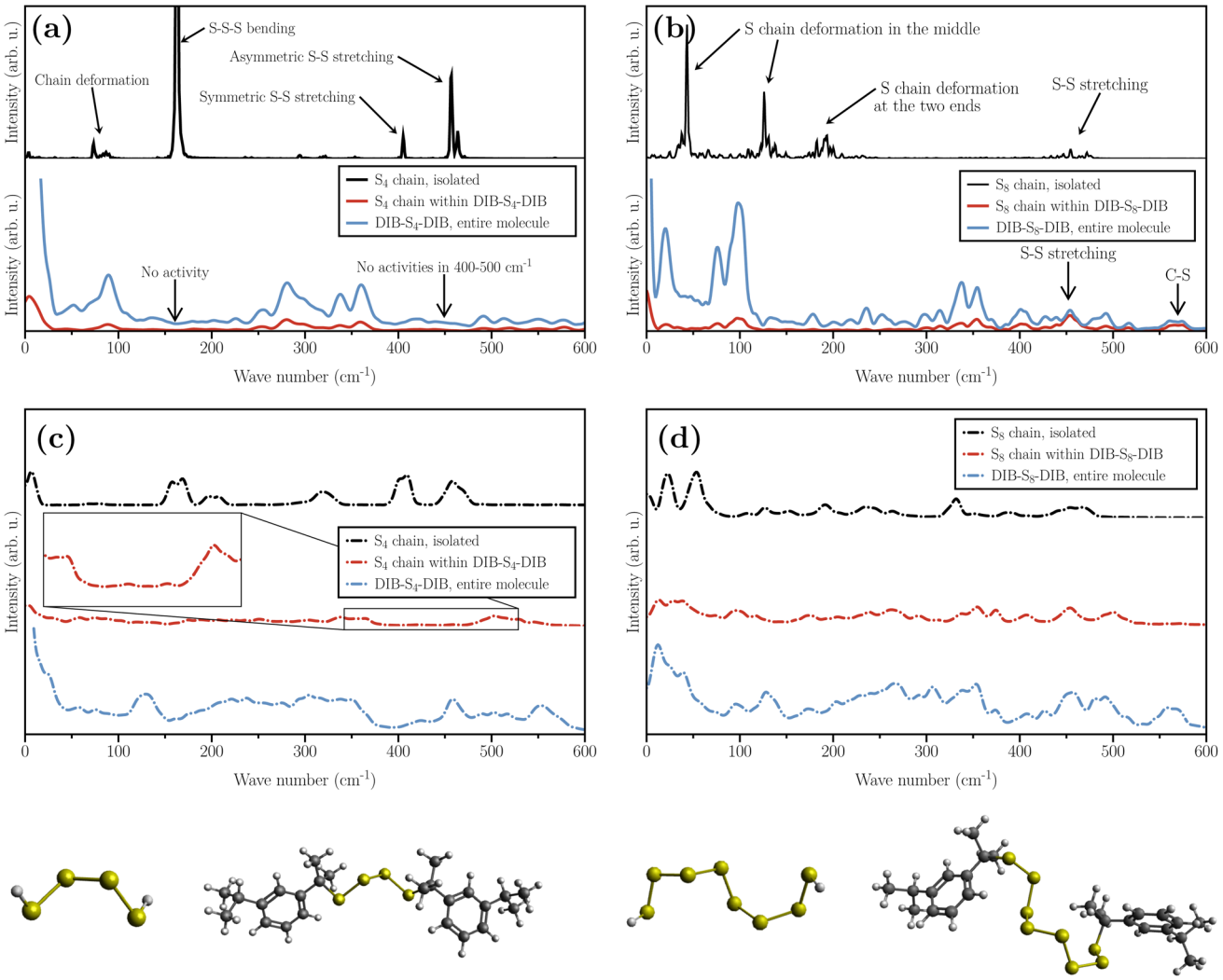

Fig. 2 Calculated Raman spectra of (a) DIB-S_4-DIB and (b) DIB-S_8-DIB in vacuum. Also shown in (a) and (b) are the computed Raman spectra of isolated S_4 and S_8 chains (black curves). Partial Raman spectra arising from sulfur chains within DIB-S_4-DIB and DIB-S_8-DIB systems are shown in red curves. (c) and (d) show the computed power spectra of DIB-S_4-DIB and DIB-S_8-DIB, respectively (blue curves). Power spectra of isolated S_4 and S_8 chains are shown in black, while partial power spectra of sulfur chains are shown in red curves. Minimum-energy structures of isolated S_4 and S_8 chains as well as those of DIB-S_4-DIB and DIB-S_8-DIB molecules are shown also in the lower panel.

in contrast to the partial power spectrum of the isolated S_4 chain, almost no activity is observed in the partial power spectrum of the S_4 chain within DIB-S_4-DIB in 400–450 cm^{-1} and below 250 cm^{-1} in Fig. 2c. However, although the low-frequency vibrations of the partial S_8 chain within DIB-S_8-DIB are insignificant, the peak corresponding to the characteristic S–S stretching vibration at 455 cm^{-1} is clearly visible [red curve in Fig. 2d].

Fig. 3 shows how the Raman peaks corresponding to the S–S stretching vibrations change as the S chain becomes longer.

In the case of S_4 chain, both peaks attributed to the symmetric and antisymmetric S–S stretching are nearly absent. As the chain length increases to six sulfur atoms in DIB-S_6-DIB, the Raman peak corresponding to the antisymmetric vibration appears, whereas that attributed to the symmetric stretching remains unnoticeable. As the S chain length further increases to S_8, both symmetric and antisymmetric peaks become distinct.

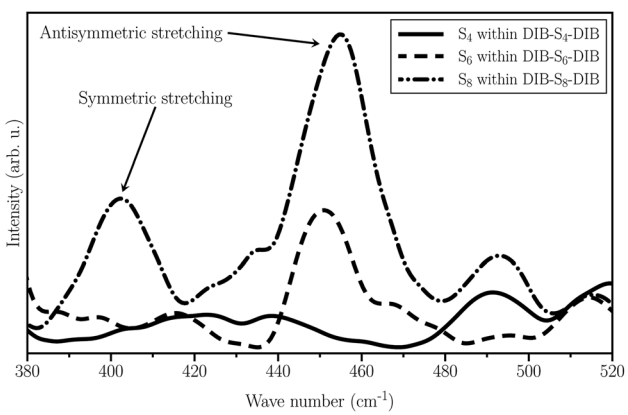

Fig. 3 Calculated partial Raman spectra of S_4, S_6, and S_8 chains in DIB-S_4-DIB, DIB-S_6-DIB, and DIB-S_8-DIB systems.

Open Access Article. Published on 18 September 2023. Downloaded on 6/18/2026 1:52:15 AM. This article is licensed under a Creative Commons Attribution-NonCommercial 3.0 Unported Licence.

Based on the above observations, we conclude that in S/DIB copolymers consisting of short S chains, the total Raman spectrum is fully dominated by the Raman activities of the organic molecules. However, in S/DIB copolymers involving longer S chains, Raman activities arising from the symmetric and antisymmetric S–S stretching vibrations in 400–500 cm^{-1} are found to be present. The observed effect has to do with the fact that polarizability of a typical S–S bond in a short S chain becomes strongly affected by the DIB molecules. The characteristic frequency for S–S stretching vibration is clearly reflected in the time-dependent variations of the spread of Wannier functions centered along S–S bonds (Fig. S1 in ESI†). Here, in order to identify differences between these time-dependent variations in short and long S chains, we calculate the autocorrelation function of the polarizability (expressed as $A = S^3$ in the Wannier polarizability method) attributed to a typical S–S bond in free S_4 and S_8 chains, as well as that in DIB-S_4-DIB and DIB-S_8-DIB molecules.

Fig. 4 shows the autocorrelation functions of S–S bond polarizabilities, $C_{AA}(t)$, in free S_n chains (black curves) and DIB-S_n-DIB (red curves) for (a) $n = 4$, and (b) $n = 8$. Although C_{AA} decays much slower in the case of free S_4 chain compared to DIB-S_4-DIB [Fig. 4a], its values for the free S_8 chain and DIB-S_8-DIB are comparable. Therefore, we conclude that the presence of massive DIB molecules leads to S–S bond polarizabilities in S/DIB copolymers containing short S chains which decline much faster than those in free S chains. However, this is not the case when the S chains are longer, and the periodic patterns in the time evolution of a typical S–S bond polarizability are found to be comparable to those in free S chains with the same length.

The observed difference in the Raman spectra can be used to distinguish between short and long sulfur chains in S/DIB copolymers, for example in the synthesis process or during cycling of the battery. To validate the above theoretical observation, first five S/DIB copolymers are synthesized with different mass fractions of DIB (and consequently varying S chain lengths) using inverse vulcanization.[3,36] Here, we refer to them as SDIBw in which w is the wt% of DIB, namely 20, 25, 30, 40, and 50%. These mass fractions correspond stoichiometrically to average chain lengths of 11, 8, 6, 4, and 3 sulfur atoms, respectively. Presence of the connection between S chains and DIB molecules is confirmed in all synthesized samples by liquid-state NMR spectroscopy while crystal formation is ruled out by X-ray diffraction measurements (see ESI†). In a second step, Raman spectra of the synthesized sulfur copolymers are measured. Fig. 5 shows a comparison between experimental Raman spectra of S/DIB copolymers with different wt% of DIB.

The intensities are normalized with respect to that of the peak at ~1000 cm^{-1} in SDIB20 sample. This peak is present in all Raman spectra and corresponds to an aromatic ring vibration. The Raman peak for the characteristic S–S stretching is

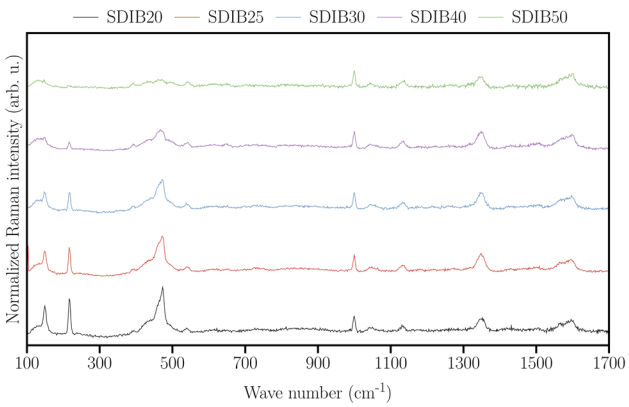

Fig. 5 Measured Raman spectra of S/DIB copolymers with different wt% of DIB.

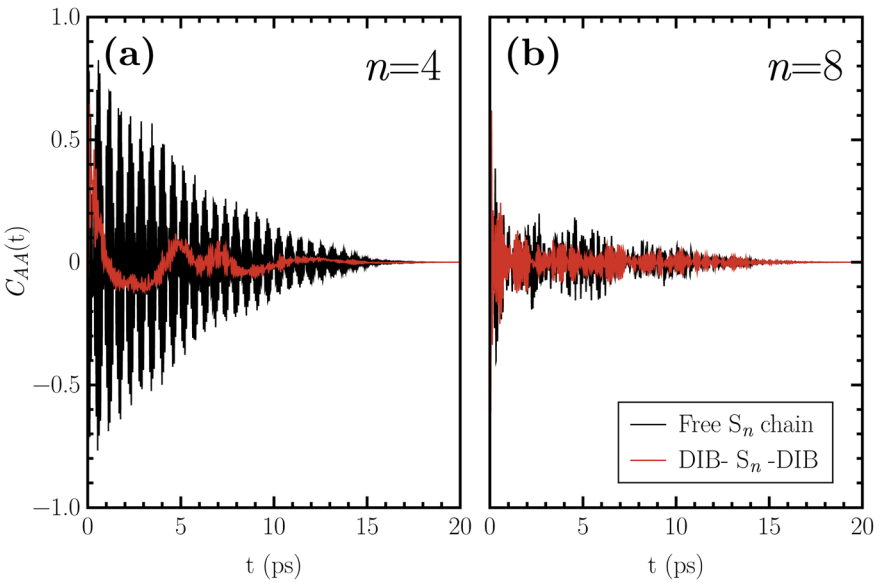

Fig. 4 Autocorrelation functions of S–S bond polarizabilities in free S_n chains (black curves) and DIB-S_n-DIB (red curves) for (a) $n = 4$, and (b) $n = 8$.

© 2023 The Author(s). Published by the Royal Society of Chemistry

Open Access Article. Published on 18 September 2023. Downloaded on 6/18/2026 1:52:15 AM.
This article is licensed under a Creative Commons Attribution-NonCommercial 3.0 Unported Licence.

observed at 473 cm^{-1}, which is about 4% higher than the theoretically predicted value. The presence of peaks in 1560–1640 cm^{-1} region indicates partially unsaturated propenyl groups. It is observed that these peaks become more intensive with increasing *w*. This is in agreement with our NMR measurements (see ESI†), where the residual C=C bonds are confirmed by the presence of NMR peaks in the range of 5.0–5.5 ppm. Nevertheless, the observed NMR peaks at chemical shift of 2.2 ppm ensure the formation of C–S bonds in all samples. The C–S bond formation is also seen in the calculated Raman spectrum of DIB-S_8-DIB in 560–575 cm^{-1} range [Fig. 2b]. In agreement with our theoretical prediction, the experimental measurements show that as the mass fraction of DIB increases (or similarly, as the average S chain length decreases), the Raman activity at around 473 cm^{-1} becomes less intensive. In a recent *in operando* FTIR study during discharge,[42] it has also been observed that the characteristic S–S stretching vibration is absent in S/DIB copolymers containing short S_n chains ($n \leq 4$) throughout discharge. However, this peak evolves as a function of cell voltage in S/DIB copolymers with longer chains, clearly indicating the formation of different Li-polysulfides. In addition, in Fig. 5 we observe Raman activities at ~165–200 cm^{-1} assigned to the sulfur chain deformation and S–S–S bending [see Fig. 2a and b], which gradually disappear with increasing wt% of DIB (shorter sulfur chains).

The Raman spectra of samples with more than 50 wt% DIB should effectively be identical to that of DIB molecules, as the only possible sulfur vibration, that is S–S stretching, is observed to be fully suppressed by the carbon moieties. Moreover, NMR analysis shows δ = 5.0–5.5 ppm, indicating the presence of unreacted propenyl groups in 1,3-diisopropenylbenzene as a monomer (see ESI†). It is therefore expected that at DIB mass fractions above 50%, Raman spectroscopic signatures of 1,3-diisopropenylbenzene monomers above 600 cm^{-1} become more prominent (Fig. 1 and S2†).

Conclusions

We have studied Raman spectra of sulfur/organic copolymers, which are presently discussed as interesting candidates for cathode materials for Li–S batteries, with a particular focus on the spectral response to variations of the length of the sulfur segments. In particular, we have chosen sulfur/1,3-diisopropenylbenzene (S/DIB) copolymers, which have recently shown a promising performance in mitigating the shuttle effect during discharge.

The comparison of quantum-chemical calculations of Raman signals with corresponding experimental spectra shows that there is a particular spectroscopic fingerprint at about 450 cm^{-1} which allows for discriminating between shorter S_n chains ($n \leq 4$) and longer ones ($n > 4$) in the copolymers at the fully charged state of the battery. This fingerprint, which corresponds to the Raman-active S–S stretching vibration, is absent in the Raman spectra of shorter sulfur chains. We attribute this effect to the confinement of shorter sulfur chains by the organic parts of the copolymer, which leads to a suppression of the net polarizability change during the vibrational motion.

It has been demonstrated that formation of short sulfur chains connecting DIB molecules are thermodynamically more favorable.[5] As a result, the initial reactions primarily occur with the shorter sulfur chains, leading to a shuttle effect reduction. It has also been observed experimentally that formation of higher-order Li-polysulfides which can dissolve in the electrolyte is largely hindered during discharge in S/DIB copolymers containing short sulfur chains.[4] Therefore, a stable cycling for 1500 cycles has been reported.[42] This clearly emphasizes the need for a strategy for the synthesis of S/DIB copolymers with controllable S chain lengths. The present study shows that Raman spectroscopy is a powerful tool to investigate structural properties of S/DIB copolymers and provides a way to probe the presence and formation of short or long sulfur chains by focusing on the frequency range attributed to the characteristic S–S vibration.

Conflicts of interest

There are no conflicts to declare.

Acknowledgements

The authors gratefully acknowledge DFG funding *via* projects PA3141/3 (Project number 420536636) and PA3141/5 (Project number 446879138). This research was also financially supported by the European Social Fund (ESF) and the State of Saxony-Anhalt through the graduate school AgriPoly. The computations have been mostly performed on a Bull Cluster at the Center for Information Services and High Performance Computing (ZIH) at TU Dresden *via* the project 'p_oligothiophenes'. We also gratefully thank Wolfgang Binder for the synthesis supervision, Karsten Busse for the XRD measurements, and Matthias Vogt for elemental analyses.

References

1 S. Evers and L. F. Nazar, New approaches for high energy density lithium–sulfur battery cathodes, *Acc. Chem. Res.*, 2013, **46**, 1135–1143.
2 X. Ji and L. F. Nazar, Advances in Li–S batteries, *J. Mater. Chem.*, 2010, **20**, 9821–9826.
3 A. G. Simmonds, J. J. Griebel, J. Park, K. R. Kim, W. J. Chung, V. P. Oleshko, J. Kim, E. T. Kim, R. S. Glass, C. L. Soles, *et al.*, Inverse vulcanization of elemental sulfur to prepare polymeric electrode materials for Li–S batteries, *ACS Macro Lett.*, 2014, **3**, 229–232.
4 A. Hoefling, D. T. Nguyen, P. Partovi-Azar, D. Sebastiani, P. Theato, S.-W. Song and Y. J. Lee, Mechanism for the Stable Performance of Sulfur-Copolymer Cathode in Lithium–Sulfur Battery Studied by Solid-State NMR Spectroscopy, *Chem. Mater.*, 2018, **30**, 2915–2923.
5 R. Kiani, D. Sebastiani and P. Partovi-Azar, On the Structure of Sulfur/1, 3-Diisopropenylbenzene Co-Polymer Cathodes for Li-S Batteries: Insights from Density-Functional Theory Calculations, *ChemPhysChem*, 2022, **23**, e202100519.

© 2023 The Author(s). Published by the Royal Society of Chemistry

Open Access Article. Published on 18 September 2023. Downloaded on 6/18/2026 1:52:15 AM.
This article is licensed under a Creative Commons Attribution-NonCommercial 3.0 Unported Licence.

6 Y. Schütze, R. de Oliveira Silva, J. Ning, J. Rappich, Y. Lu, V. G. Ruiz, A. Bande and J. Dzubiella, Combined first-principles statistical mechanics approach to sulfur structure in organic cathode hosts for polymer based lithium–sulfur (Li–S) batteries, *Phys. Chem. Chem. Phys.*, 2021, **23**, 26709–26720.

7 Y. Schütze, D. Gayen, K. Palczynski, R. de Oliveira Silva, Y. Lu, M. Tovar, P. Partovi-Azar, A. Bande and J. Dzubiella, How Regiochemistry Influences Aggregation Behavior and Charge Transport in Conjugated Organosulfur Polymer Cathodes for Lithium–Sulfur Batteries, *ACS Nano*, 2023, **17**(8), 7889–7900.

8 R. Zou, W. Liu and F. Ran, Sulfur-containing polymer cathode materials: From energy storage mechanism to energy density, *InfoMat*, 2022, e12319.

9 S. Park, S.-J. Kim, Y.-E. Sung, K. Char and J. G. Son, Short-chain polyselenosulfide copolymers as cathode materials for lithium–sulfur batteries, *ACS Appl. Mater. Interfaces*, 2019, **11**, 45785–45795.

10 S. Diez, A. Hoefling, P. Theato and W. Pauer, Mechanical and electrical properties of sulfur-containing polymeric materials prepared *via* inverse vulcanization, *Polymers*, 2017, **9**, 59.

11 F. Zhao, Y. Li and W. Feng, Recent Advances in Applying Vulcanization/Inverse Vulcanization Methods to Achieve High-Performance Sulfur-Containing Polymer Cathode Materials for Li–S Batteries, *Small Methods*, 2018, **2**, 1800156.

12 A. S. M. Ghumman, M. M. Nasef, M. R. Shamsuddin and A. Abbasi, Evaluation of properties of sulfur-based polymers obtained by inverse vulcanization: Techniques and challenges, *Polym. Polym. Compos.*, 2021, **29**, 1333–1352.

13 M. Hagen, P. Schiffels, M. Hammer, S. Dörfler, J. Tübke, M. Hoffmann, H. Althues and S. Kaskel, In-situ Raman investigation of polysulfide formation in Li-S cells, *J. Electrochem. Soc.*, 2013, **160**, A1205.

14 H.-L. Wu, L. A. Huff and A. A. Gewirth, In situ Raman spectroscopy of sulfur speciation in lithium–sulfur batteries, *ACS Appl. Mater. Interfaces*, 2015, **7**, 1709–1719.

15 P. Partovi-Azar, T. D. Kühne and P. Kaghazchi, Evidence for the existence of Li 2 S 2 clusters in lithium–sulfur batteries: *ab initio* Raman spectroscopy simulation, *Phys. Chem. Chem. Phys.*, 2015, **17**, 22009–22014.

16 D. Blanchard and M. Slagter, operando Raman and optical study of lithium polysulfides dissolution in lithium–sulfur cells with carrageenan binder, *JPhys Energy*, 2021, **3**, 044003.

17 J. Wang, R. M. Wolf, J. W. Caldwell, P. A. Kollman and D. A. Case, Development and testing of a general amber force field, *J. Comput. Chem.*, 2004, **25**, 1157–1174.

18 J. D. Gale, Empirical potential derivation for ionic materials, *Philos. Mag. B*, 1996, **73**, 3–19.

19 J. D. G. U. L. P. Gale, A computer program for the symmetry-adapted simulation of solids, *J. Chem. Soc., Faraday Trans.*, 1997, **93**, 629–637.

20 J. D. Gale and A. L. Rohl, The general utility lattice program (GULP), *Mol. Simul.*, 2003, **29**, 291–341.

21 C. I. Bayly, P. Cieplak, W. Cornell and P. A. Kollman, A well-behaved electrostatic potential based method using charge restraints for deriving atomic charges: the RESP model, *J. Phys. Chem.*, 1993, **97**, 10269–10280.

22 D. Golze, J. Hutter and M. Iannuzzi, Wetting of water on hexagonal boron nitride@ Rh (111): a QM/MM model based on atomic charges derived for nano-structured substrates, *Phys. Chem. Chem. Phys.*, 2015, **17**, 14307–14316.

23 C. Campañá, B. Mussard and T. K. Woo, Electrostatic potential derived atomic charges for periodic systems using a modified error functional, *J. Chem. Theory Comput.*, 2009, **5**, 2866–2878.

24 S. Nosé, A unified formulation of the constant temperature molecular dynamics methods, *J. Chem. Phys.*, 1984, **81**, 511–519.

25 W. G. Hoover, Canonical dynamics: Equilibrium phase-space distributions, *Phys. Rev. A*, 1985, **31**, 1695.

26 T. D. Kühne, M. Iannuzzi, M. Del Ben, V. V. Rybkin, P. Seewald, F. Stein, T. Laino, R. Z. Khaliullin, O. Schütt, F. Schiffmann, *et al.*, CP2K: An electronic structure and molecular dynamics software package-Quickstep: Efficient and accurate electronic structure calculations, *J. Chem. Phys.*, 2020, **152**, 194103.

27 J. VandeVondele and J. Hutter, Gaussian basis sets for accurate calculations on molecular systems in gas and condensed phases, *J. Chem. Phys.*, 2007, **127**, 114105.

28 J. P. Perdew, K. Burke and M. Ernzerhof, Generalized gradient approximation made simple, *Phys. Rev. Lett.*, 1996, **77**, 3865.

29 S. Goedecker, M. Teter and J. Hutter, Separable dual-space Gaussian pseudopotentials, *Phys. Rev. B: Condens. Matter Mater. Phys.*, 1996, **54**, 1703.

30 M. Krack, Pseudopotentials for H to Kr optimized for gradient-corrected exchange-correlation functionals, *Theor. Chem. Acc.*, 2005, **114**, 145–152.

31 S. Grimme, J. Antony, S. Ehrlich and H. Krieg, A consistent and accurate *ab initio* parametrization of density functional dispersion correction (DFT-D) for the 94 elements H-Pu, *J. Chem. Phys.*, 2010, **132**, 154104.

32 P. Partovi-Azar and T. D. Kühne, Efficient "On-the-Fly" calculation of Raman Spectra from *Ab-Initio* molecular dynamics: Application to hydrophobic/hydrophilic solutes in bulk water, *J. Comput. Chem.*, 2015, **36**, 2188–2192.

33 P. Partovi-Azar and T. D. Kühne, Full Assignment of *Ab-Initio* Raman Spectra at Finite Temperatures Using Wannier Polarizabilities: Application to Cyclohexane Molecule in Gas Phase, *Micromachines*, 2021, **12**, 1212.

34 M. Brehm and B. Kirchner, TRAVIS-a free analyzer and visualizer for Monte Carlo and molecular dynamics trajectories, *J. Chem. Inf. Model.*, 2011, **51**(8), 2007–2023.

35 M. Brehm, M. Thomas, S. Gehrke and B. Kirchner, TRAVIS—A free analyzer for trajectories from molecular simulation, *J. Chem. Phys.*, 2020, **152**, 164105.

36 W. J. Chung, J. J. Griebel, E. T. Kim, H. Yoon, A. G. Simmonds, H. J. Ji, P. T. Dirlam, R. S. Glass, J. J. Wie, N. A. Nguyen, *et al.*, The use of elemental sulfur as an alternative feedstock for polymeric materials, *Nat. Chem.*, 2013, **5**, 518–524.

© 2023 The Author(s). Published by the Royal Society of Chemistry

Open Access Article. Published on 18 September 2023. Downloaded on 6/18/2026 1:52:15 AM.
This article is licensed under a Creative Commons Attribution-NonCommercial 3.0 Unported Licence.

37 A. J. Berndt, J. Hwang, M. D. Islam, A. Sihn, A. M. Urbas, Z. Ku, S. J. Lee, D. A. Czaplewski, M. Dong, Q. Shao, *et al.*, Poly (sulfur-random-(1, 3-diisopropenylbenzene)) based mid-wavelength infrared polarizer: optical property experimental and theoretical analysis, *Polymer*, 2019, **176**, 118–126.

38 John Wiley & Sons, I. SpectraBase, *SpectraBase Compound ID=IkqI6N7Ayh0 SpectraBase Spectrum ID=JDXWPt9E2Qb*, 2022, **https://spectrabase.com/spectrum/JDXWPt9E2Qb**.

39 John Wiley & Sons, I. SpectraBase; *SpectraBase Compound ID=IrmpzL3iJ1K SpectraBase Spectrum ID=1uL7oZa5Ssu*, 2022, **https://spectrabase.com/spectrum/1uL7oZa5Ssu**.

40 D. Lin-Vien, N. B. Colthup, W. G. Fateley and J. G. Grasselli, *The handbook of infrared and Raman characteristic frequencies of organic molecules*, Elsevier, 1991.

41 J. Plaickner, E. Speiser, S. Chandola, N. Esser and D. K. Singh, Adsorption of toluene-3, 4-dithiol on silver islands investigated by surface-enhanced Raman spectroscopy, *J. Raman Spectrosc.*, 2020, **51**, 788–794.

42 A. Rafie, R. Pereira, A. A. Shamsabadi and V. Kalra, *In Operando* FTIR Study on the Effect of Sulfur Chain Length in Sulfur Copolymer-Based Li–S Batteries, *J. Phys. Chem. C*, 2022, **126**, 12327–12338.